

# THREE-DIMENSIONAL MULTI-BODY BOND GRAPH MODEL FOR VIBRATION CONTROL OF LONG SHAFTS – APPLICATION TO OILWELL DRILLING

D. Geoff Rideout<sup>(a)</sup>, Farid Arvani<sup>(b)</sup>, Stephen D. Butt<sup>(c)</sup>, Ehsan Fallahi<sup>(d)</sup>

Advanced Drilling Group, Faculty of Engineering and Applied Science  
Memorial University  
St. John's, NL Canada A1B 3X5

<sup>(a)</sup>[g.rideout@mun.ca](mailto:g.rideout@mun.ca), <sup>(b)</sup>[f.arvani@mun.ca](mailto:f.arvani@mun.ca), <sup>(c)</sup>[sdbutt@mun.ca](mailto:sdbutt@mun.ca), <sup>(d)</sup>[e.fallahi@mun.ca](mailto:e.fallahi@mun.ca)

## ABSTRACT

During oilwell drilling, the long slender drillstring is susceptible to coupled lateral, axial and torsional vibrations that can reduce drilling efficiency and damage components. A bond graph model of an 80 metre drillstring collar section, subjected to bit-rock interaction boundary conditions and multiple lateral stabilizers, is created. Three-dimensional rigid lumped segments are connected by axial, torsional, shear, and bending springs. Thirty segments are sufficient to predict the lowest natural frequencies and static deflection accurately. An active lateral vibration controller is implemented, in which actuators and strain gauges are placed 90-degrees apart around the pipe walls, near the middle of the longest span. A proportional controller acting on the strain gauge output significantly attenuates vibration. The model structure allows easy reconfiguration of the drillstring geometry, boundary conditions, and actuator and sensor locations, to study the effect of any controller on coupled lateral, axial, and/or torsional vibration.

Keywords: multibody dynamics, bond graph, lumped segment, drillstring, lateral vibration control

## 1. INTRODUCTION

Drilling accounts for approximately 35% of all oil and gas exploration and production costs (CAPP, 2012). An estimated 2% to 10% of well drilling costs can arise from vibration-related problems, such as lost time while pulling out of hole, reduced rate of penetration (ROP), poor wellbore quality, and increased service cost because of the need for ruggedized equipment (Jardine et al., 1994). Figure 1 shows a schematic of a drillstring. The drill pipes form a long slender beam-like structure in tension. The bottom-hole assembly (BHA) consists of heavier pipes called collars, shock absorbers ("shock subs"), the bit, and possibly vibrating tools and measurement-while-drilling (MWD) tools for logging vibration levels and reporting orientation in deviated (non-vertical) wells. A "neutral point" between tension and compression is typically near the top of the BHA. Stabilizers provide low radial clearance at certain points, potentially creating multiple

spans for lateral vibration. Stabilizers are typically modeled as pinned lateral boundary conditions.

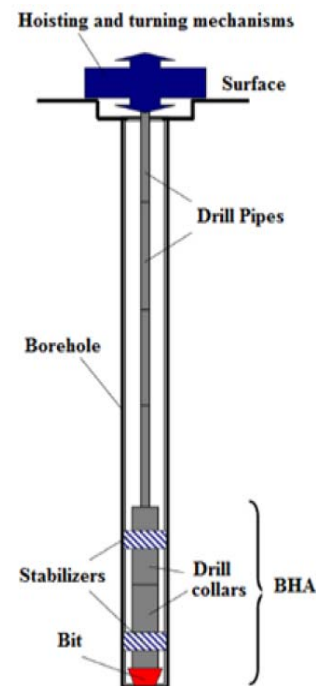


Figure 1: Drillstring Schematic (Khulief et al., 2007)

Potentially destructive vibration can occur axially, torsionally, or laterally. The most severe manifestations of these are, respectively,

- bit bounce where the bit comes off bottom despite weight on bit (WOB) from collars
- stick slip where the bit alternately stops and overspeeds
- severe lateral forward or backward whirl with wellbore contact

While many approaches to drillstring modeling have been pursued, there are few models that can capture axial, torsional and lateral vibration without prohibitively high computation time. Most models capture a subset of the three types of vibration, and may

neglect coupling. Control design is typically done on overly simple models. Verifying the performance of the controller by including sensors and actuators in a more complex finite element or modal expansion model can be difficult. This paper presents a physically intuitive multibody bond graph model that predicts three-dimensional drillstring (or any other long shaft) vibratory motion, and into which a controller and associated components can be easily added. A simple lateral vibration controller, effected by axial force actuators, is demonstrated.

## 2. LITERATURE REVIEW

Active control of drillstring vibration is an emerging research area. Linear quadratic regulator (LQR) control of torsional vibration has been simulated by Yigit and Christoforou (2006) and Sarker et al. (2012), with torsional control action having a positive effect on axial vibration. Lumped segment models with axial and torsional degrees of freedom, coupled through a bit-rock interaction model, were used. Stick-slip control has been simulated using robust  $\mu$ -synthesis (Karkoub et al., 2010),  $H_\infty$  control (Serrarens et al., 1998), genetic algorithms (Karkoub et al., 2009), torque estimators (Pavkovic et al., 2011), and modeling error compensation-based control (Puebla and Alvarez-Ramirez, 2008). These controllers were designed using simple two-mass torsional pendulum models.

Many such controllers have practical limitations, most notably the difficulty in measuring states such as instantaneous bit speed. While measurement-while-drilling (MWD) tools exist for recording accelerations, force and torque near the bit, there is no reliable and cost-effective means for delivering this information, at a suitable sampling frequency, to a controller at the surface. A "Soft Torque Rotary System" (Jansen and Van den Steen, 1995), which has been adopted by industry, controls top drive speed to absorb torsional waves, based on torque feedback. Rotary vibration control is most common in industry because of the relative ease of detecting torque fluctuations at the surface. Active lateral and axial control is not currently done. In other applications such as bridges (Younesian et al., 2010) and cantilever beams (Ahmadabadi and Khadem, 2012), lateral vibration has been suppressed by elements such as nonlinear energy sinks; however, the structures are not rotating shafts. In drilling, lateral vibration control is done indirectly, through control of parameters such as rotary speed to avoid lateral resonance frequencies.

The rotating shaft can be modeled using simple one-dimensional decoupled lumped-segment or modal expansion approaches (Karnopp et al., 2006) for axial, torsional, and lateral motion. While axial-torsional coupling can be done through bit-rock interaction models, the coupling of lateral vibration to axial and torsional is more difficult. Energy methods (Lagrangian, Hamiltonian) have been used to analytically determine equations of motion, which have been solved with approximate methods (Yigit and

Christoforou, 1996, Ghasemloonia et al., 2012). Reconfiguring such models for different and new boundary conditions (e.g., more spans between stabilizers), and new discrete components such as vibrating tools, shock absorbers, and actuators is neither obvious nor trivial. Finite element models, for example (Ghasemloonia et al., 2013, Khulief and Al-Naser, 2005), can be more easily reconfigured, but typically exhibit high computation times and are not suited to prediction of closed-loop dynamic response.

This paper describes a bond graph model in which three-dimensional rigid lumped segments are connected by axial, torsional, shear, and bending springs. The model is demonstrated to capture coupled axial, lateral and torsional vibrations at the appropriate natural frequencies. Boundary conditions, including wellbore contact, location of stabilizers, and bit rock force or displacement can be reconfigured. The bond graph formalism and modeling approach allow straightforward inclusion of actuator or sensor submodels. Implementation of a controller directly on to the bond graph is done in commercial software. A lateral vibration suppression controller case study is presented.

## 3. MODEL DESCRIPTION

The drillstring is represented as a sequence of cylindrical rigid bodies joined by spherical joints with three translational and rotational compliances, as shown in Figure 2. Springs " $k_{bend}$ " are rotary springs about the body-fixed  $x$  and  $y$  axes of body  $i+1$ , " $k_{tors}$ " is a rotary spring about body-fixed  $z$ , " $k_{axial}$ " is a translational spring in body-fixed  $z$ , and " $k_{shear}$ " are translational springs in body-fixed  $x$  and  $y$ . The torsional and bending springs are shown separately in the right portion of the figure, and one shear spring is not shown for clarity; however, all springs exist at the joint between point B on body  $i$  and Point A on body  $i+1$ .

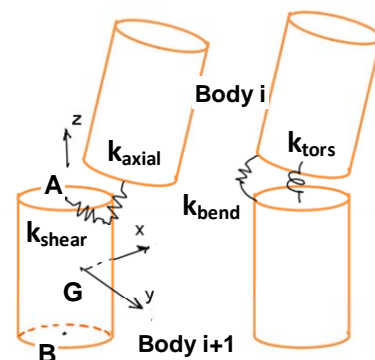


Figure 2: Successive Multibody Segments

Stiffness values are computed for a segment length  $\Delta x = L/n$  of a string of length  $L$  with  $n$  segments, using basic solid mechanics theory, as follows (Karnopp et al., 2006):

$$\begin{aligned}
k_{\text{axial}} &= EA/\Delta X \\
k_{\text{torsion}} &= GJ/\Delta X \\
k_{\text{bend}} &= EI/\Delta X \\
k_{\text{shear}} &= \kappa AG/\Delta X
\end{aligned}
\quad (1-4)$$

where  $E$  is elastic modulus,  $A$  and  $I$  are cross-sectional area and area moment,  $G$  is modulus of rigidity,  $J$  is polar moment of area, and  $\kappa$  is a parameter accounting for non-uniform shear across a cross section.

### 3.1. Bond Graph of Segments and Joints

The Euler Junction Structure is used, representing the following equations governing the dynamics of bodies undergoing large motions (Karnopp et al., 2006):

$$\Sigma^0 \bar{F} = d/dt (\bar{m}^0 \bar{v}_{Gi}) = \bar{m}^0 \dot{\bar{v}}_{Gi} \quad (5-6)$$

$$\Sigma^i \bar{M} = d/dt (\bar{J}^i \bar{\omega}_i) = \bar{J}^i \dot{\bar{\omega}}_i + {}^i \bar{\omega}_i \times \bar{J}^i \bar{\omega}_i$$

where  $G$  is the mass centre, left superscript  $\theta$  indicates vectors resolved into inertial frame components, and  $i$  indicates vectors (in this case, absolute velocities) resolved along body-fixed frame  $i$ . The translational equations are expressed in frame  $\theta$  to facilitate application of the gravity vector. The first term on the right hand side of the rotational equation is an inertial term, and the second term gyrational. The hinge point  $A$  velocity is defined as follows ( $B$  is defined similarly):

$${}^1 \bar{v}_{Ai} = {}^1 \bar{v}_{Gi} + {}^1 \bar{v}_{Ai/Gi} \quad (7-8)$$

$${}^1 \bar{v}_{Ai/Gi} = {}^i \bar{\omega}_i \times {}^i \bar{r}_{Ai/Gi} = {}^i \tilde{r}_{Ai/Gi} {}^i \bar{\omega}_i$$

where  ${}^i \bar{r}_{Ai/Gi}$  is the position vector from  $G$  to  $A$ , and  ${}^i \tilde{r}_{Ai/Gi}$  is a skew-symmetric matrix containing the relative position vector components.

Figure 3 is a top-level vector bond graph (Breedveld, 1985) representation of the above equations. Note the modulated transformer representation of Eq'n (8). Cardan orientation angle (rotations  $\psi$ ,  $\theta$ ,  $\phi$  about body fixed  $z$ ,  $y$ ,  $x$ ) rates are calculated, integrated, and used to create rotation matrices between body-fixed and inertial coordinate frames according to the following equations:

$$\begin{aligned}
\dot{\theta} &= \cos \phi \omega_y - \sin \phi \omega_z \\
\dot{\psi} &= \frac{\sin \phi}{\cos \theta} \omega_y + \frac{\cos \phi}{\cos \theta} \omega_z
\end{aligned}
\quad (9-11)$$

$$\dot{\phi} = \omega_x + \sin \phi \frac{\sin \theta}{\cos \theta} \omega_y + \cos \phi \frac{\sin \theta}{\cos \theta} \omega_z$$

Orthogonal rotation matrices transform vector components as follows:

$${}^0 \bar{v} = R_i^0 {}^i \bar{v}, {}^i \bar{v} = R_0^i {}^0 \bar{v}, R_0^i = [R_i^0]^T \quad (12)$$

The rotation matrix, as a function of Cardan angles, is:

$$R_i^0 = \begin{bmatrix} c_\theta c_\psi & -c_\theta s_\psi & s_\theta \\ c_\phi s_\psi + s_\phi s_\theta c_\psi & c_\phi c_\psi - s_\phi s_\theta c_\psi & -s_\phi c_\theta \\ s_\phi s_\psi - c_\phi s_\theta c_\psi & s_\phi c_\psi + c_\phi s_\theta c_\psi & c_\phi c_\theta \end{bmatrix} \quad (12)$$

where “ $c$ ” and “ $s$ ” represent  $\cos$  and  $\sin$  respectively.

Figure 4 shows a joint submodel in which the relative velocity between point B and A on successive bodies is calculated in the Body  $i+1$ -fixed frame. The multiport C and R elements have a diagonal stiffness matrix to model the stiffnesses described in Eq'ns (1-4), and a viscous material damping matrix tuned to give a reasonable damping ratio in the first mode.

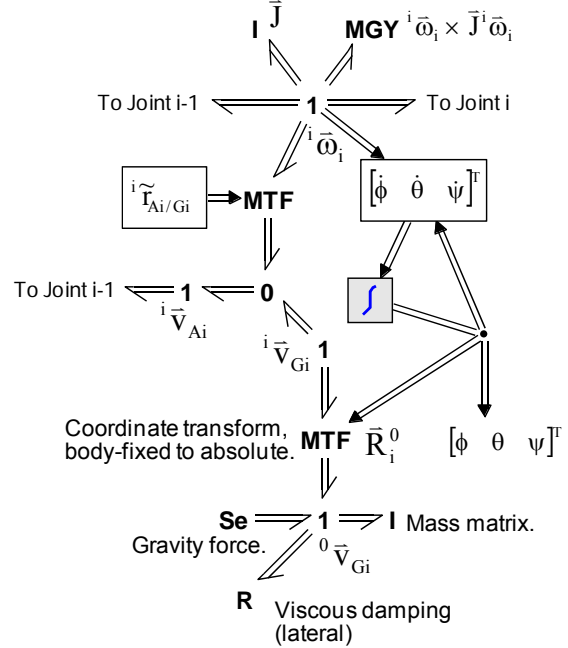


Figure 3 – Body  $i$  Bond Graph

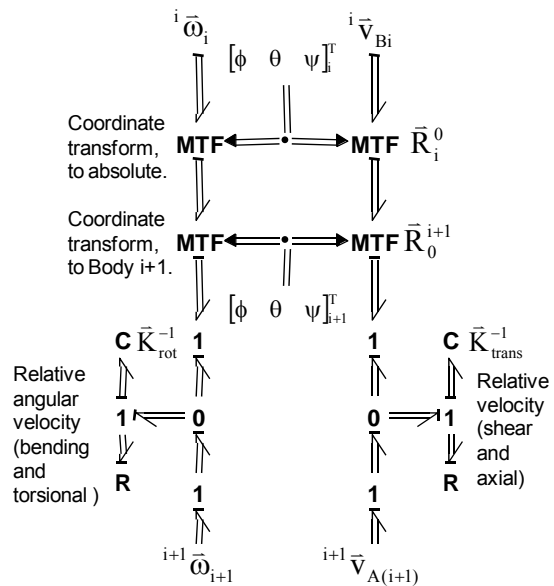


Figure 4 – Joint  $i$  Bond Graph

The 80-m collar section under study is very similar to the schematic shown in Figure 1. The top is constrained axially and laterally with stiff translational springs, and a rotational speed increasing from 0 to 20 rad/s over 1 second is prescribed. Stabilizers are modeled via stiff lateral constraint springs at the bit, and 26.67 m above the bit. A 3 mm sinusoidal axial bit displacement boundary condition is applied, at a frequency equal to rotational speed. The pipe is divided into 30 segments of equal length.

### 3.2. Modeling Wellbore Contact

Use of lumped segments, rather than energy methods, simplifies the inclusion of wellbore contact. Assuming a radial clearance of 2 cm between the collars and wellbore, stiff springs with discontinuous constitutive laws provide no effort until the radial deflection exceeds 2 cm at Bodies 11 and 26, which are at the middle of their respective spans and thus most likely to collide with the borehole. The velocities of points  $G_{11}$  and  $G_{26}$  are expressed in the inertial frame, and integrated to determine their position and then angle, so that the wellbore contact spring force can be directed along that angle. The spring is linear, with an arbitrary high stiffness value of  $10^7$  N/m. This value can be refined, given knowledge of the specific rock type for uncased wells, or using contact mechanics models of steel-on-steel for wells with a steel casing sleeve surrounding the drillstring. The contact model does not include rubbing friction. Future work will add such friction in addition to elastic restoring force, so that forward and backward whirl can be predicted. Detection of wellbore contact and computation of force and angle are done using the following equations.

$$\delta = \sqrt{X^2 + Y^2}$$

$$\phi = \tan^{-1}(Y/X) \quad (14-17)$$

$$F = k_w(\delta - \delta_0)$$

$$F_x = F \cos \phi, F_y = F \sin \phi$$

where  $\delta$  is radial deflection,  $\delta_0$  is maximum wellbore clearance,  $X$  and  $Y$  are absolute coordinates of the centre of gravity,  $F$  and  $k_w$  are contact force and stiffness, and  $\phi$  is angle between the wellbore centre and the inertial  $X$  axis. See Figure 5.

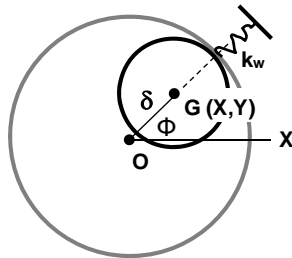


Figure 5 – Wellbore Contact Schematic

### 3.3. Modeling Sensors and Actuation

Strain on the outer surface of the pipe is assumed to correlate to bending stress, and is thus used as the input to the lateral vibration controller. Two pairs of actuators are modeled at the midpoints of the two spans. Figure 6 shows actuators that work as follows: positive tensile strain at point  $C$  results in the controller applying a compressive force to expand the distance between points  $D$  on adjacent bodies. An equal and opposite tensile force is applied at points  $C$  to create a moment about body-fixed  $y$  that opposes bending stress. Similarly, actuators at  $E$  and  $F$  will create a moment in response to strain at  $E$ .

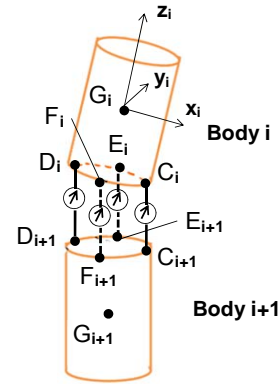


Figure 6 – Actuator Location Detail

Strain at  $C$  is assumed proportional to the state (torsional deflection) of the bending spring component in the body-fixed  $y$  direction as shown in Figure 7. Lateral vibration-induced strain is assumed to be much larger than axial deformation strain.

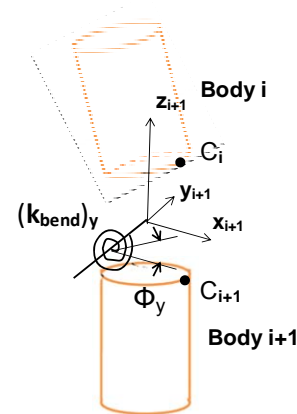


Figure 7 – Tensile Strain Computed at Points  $C$

Combining Hooke's Law, Eq'n (3), and the relation between bending moment and beam curvature, the proportionality constant between spring state and strain is derived.

$$\varepsilon = \frac{\sigma}{E} = \frac{Mr}{EI} = \frac{r}{EI} \left( EI \frac{d\phi}{dx} \right) \quad (18)$$



#### 4.1. Controller Performance

Actuators are placed near the midpoints of both the long and short spans. Figure 11 compares the onset of lateral vibration at the long span midpoint with and without the controller. The upper plot is uncontrolled, showing vibration peaking at 15 mm radial displacement and arriving at a steady-state level of approximately  $8 \pm 5$  mm. The middle plot is with the high-gain proportional controller that allows each actuator to apply unlimited compressive or tensile forces. The unrestricted actuator force approaches 5000 N, with low power requirements as shown in Figure 12. A simulated actuator that could only generate compressive forces, and is restricted to 5000 N, generates the vibration shown in the lower plot of Figure 11. Figure 13 compares power output for the unrestricted and restricted actuators. The actuators must provide power equal to the magnitude of the values in Figure 13 (negative power refers to effort and velocity in opposite directions). The model indicates that restricting actuation direction and peak force significantly decreases control effect while increasing power requirements. Results for actuators *C-D* are shown, but actuators *E-F* behave similarly.

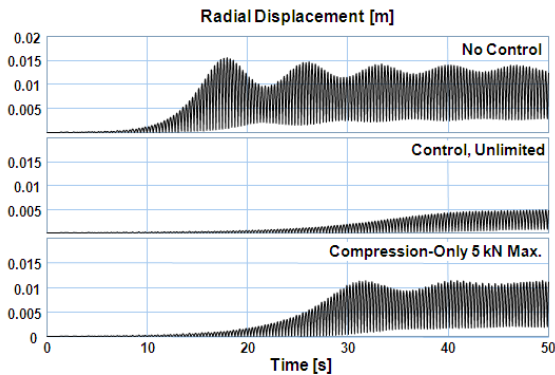


Figure 11 – Open- and Closed-Loop Vibration Levels, System Starting From Rest

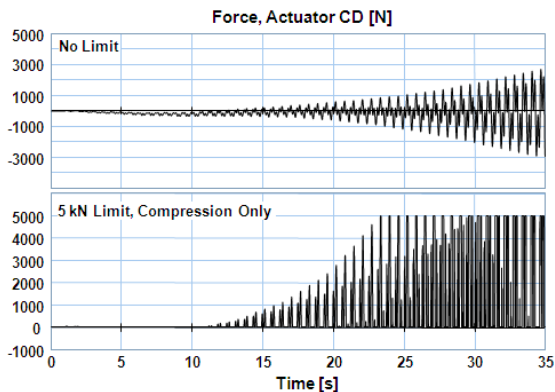


Figure 12 – Actuator Force

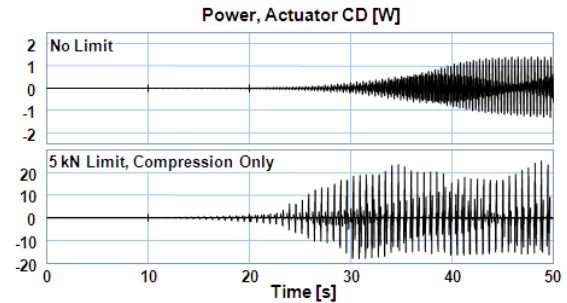


Figure 13 – Actuator Power

If the controller is switched on during steady-state uncontrolled vibration, the radial deflection of both spans is reduced as shown in Figure 14. Top span vibration is reduced, strain is dramatically reduced, actuator power peaks at a higher value of 400 W compared to when control is initiated at startup; and peak actuator force (not shown) is 26 kN. Radial deflection of the bottom span is reduced slightly, but is small even without control.

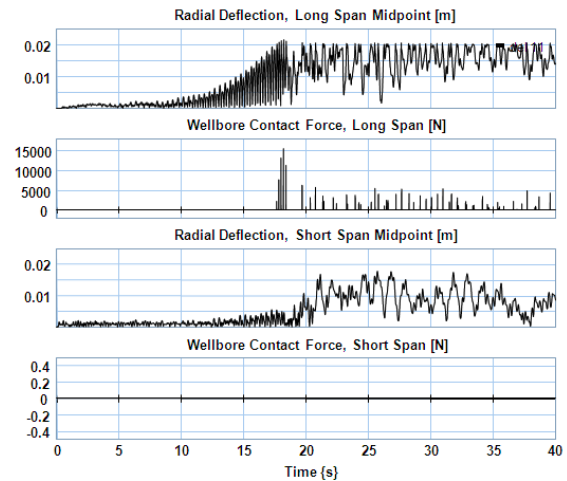


Figure 14 – Controller Switched On After 25 Seconds

#### 4.2. Discussion

The use of only two actuators, one on each span, results in high proportional gains and very few actuation sites. While the controller is stable for the scenarios shown, it exhibits instability when actuator delays are introduced. Lowering gains to  $10^6$  restores stability, but control benefit is lost. Figure 14 shows that vibration is not reduced in proportion to strain near the actuator, when only one actuator per span is used. This underactuation means that it is possible to reduce strain, say at point *C* in the middle of the long top span, to zero without restoring the radial position of the cross section to the middle of the wellbore. The actuator can create a local region of zero bending in a pipe section that is pressed against the wellbore, and subjected to rubbing and repeated collision forces. Figure 15 shows such behavior when the controller is switched on during a more severe vibration than in Figure 14. Figures 15 and 16 show repeated and prolonged excursions of the pipe

to the wellbore wall for both spans, and no reduction of vibration despite reduction of strain. More actuation sites, with lower gains, are suggested by the model in order to stably control lateral motion using strain feedback.

The separate controllers for the two orthogonal lateral directions are, in this preliminary study, single input-single output. More sophisticated controller design would require a study of the coupling between the orthogonal modes and the potential benefits of a multiple-input approach to the design and tuning of each controller.

A three-dimensional model, as opposed to a planar model, is necessary for exploratory simulations of the potential of a vibration suppression system such as the strain-based proportional feedback controller. Axial and lateral vibrations could be studied in a decoupled manner by simple modal expansion or lumped segment models, and a multibody approach could be done much more simply with motion restricted to a single lateral plane, to simulate strain-feedback actuation. However, the rotation of a drillstring or similar shaft introduces centrifugal excitations and moves the actuators in and out of a given lateral plane. The model described herein is a physically intuitive and easily-reconfigured representation of a rotating beam with the required three dimensions.

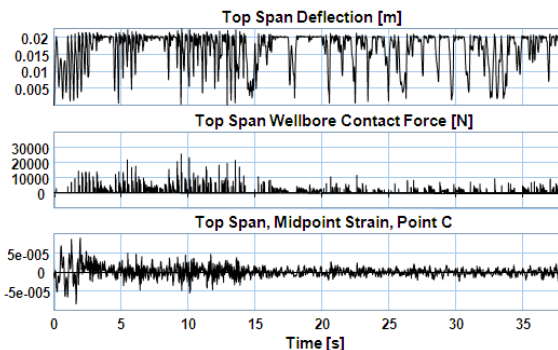


Figure 15 – Controller Pushing Pipe into Wellbore, Top Span

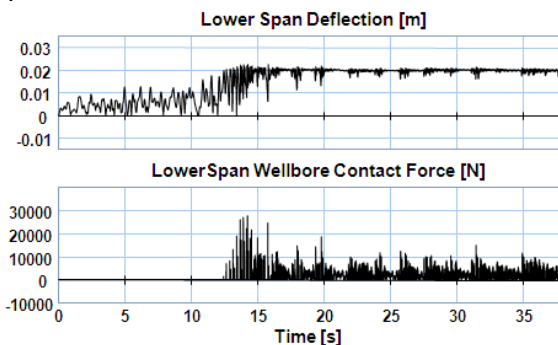


Figure 16 – Controller Pushing Pipe into Wellbore, Top Span

## 5. CONCLUSIONS AND FUTURE WORK

A rotating shaft, in this application an oilwell drillstring, has been modeled using a succession of rigid

bodies moving in three dimensions and constrained by shear, torsional, bending, and axial stiffness elements. Thirty segments are used to model a two-span rotating beam with a bit-rock displacement axial boundary condition, rotating unbalance, and contact with an exterior surface (wellbore) at the midpoint of each span. The model is useful not only for predicting coupled axial, torsional, and lateral vibrations due to unbalance or external excitation, but also for preliminary design and implementation of vibration controllers. Mid-span strain gauges and actuators are simulated, with high-gain proportional feedback showing potential for vibration suppression. The model indicates that more than two actuation sites are required, to prevent the actuators from locally straightening the shaft to eliminate bending strain without reducing lateral deflection. The model is easily reconfigurable to study alternate control strategies such as active unbalance masses that could apply transverse control forces more directly. Future work will be directed towards more robust control using these two approaches, as well as validating the model against finite element models and measured data from actual oil wells. Important model extensions include sliding friction from wellbore contact, fluid friction, and a bit-rock interaction submodel to predict axial displacement and reaction torque with higher fidelity.

## ACKNOWLEDGEMENTS

This work was done at the Advanced Exploration Drilling Technology Laboratory at Memorial University in St. John's, Canada. Financial support was provided by Husky Energy, Suncor Energy, Newfoundland and Labrador Research and Development Corporation, and Atlantic Canada Opportunities Agency under AIF contract number 781-2636-192049.

## REFERENCES

- Ahmadabadi, Z. N., and Khadem, S.E., 2012. Nonlinear vibration control of a cantilever beam by a nonlinear energy sink. *Mech. and Machine Theory*, 50, 134-149.
- Breedveld, P.C., 1985. Proposition for an unambiguous vector bond graph notation. *Journal of Dynamic Systems, Measurement and Control*. 104 (3), 267-270.
- Canadian Association of Petroleum Producers (CAPP), 2012. *Compiled Industry Statistics 1981-2011*.
- Ghasemloonia, A., Rideout, D. G., and Butt, S. D., 2012. Coupled Transverse Vibration Modeling of Drillstrings Subjected to Torque and Spatially Varying Axial Load, *Journal of Mechanical Engineering Science (IMEchE, Part C)*. 227 (5), 946-960.
- Ghasemloonia, A, Rideout D. G. and Butt, S. D., 2013. Vibration Analysis of a Drillstring in Vibration-Assisted Rotary Drilling: Finite Element Modeling With Analytical Validation. *ASME Journal of Energy Resources Technology*, 135 (3).

- Jardine, S., Malone, D., and Sheppard, M., 1994. Putting a Damper on Drilling's Bad Vibration, *Oilfield Review*, 6 (1), January.
- Jansen, J.D., and Van den Steen, L., 1995. Active Damping of Self-Excited Torsional Vibrations in Oil Well Drillstrings. *Journal of Sound and Vibration*, 179 (4), 647-668.
- Karkoub, M., Abdel-Magid, Y. L., and Balachandran, B., 2009. Drill-string Torsional Vibration Suppression Using GA Optimized Controllers. *Journal of Canadian Petroleum Technology*, 48 (12), 32-38.
- Karkoub, M., Zribi, M., Elchaar, L., and Lamont, L., 2010. Robust  $\mu$ -Synthesis Controllers for Suppressing Stick-slip Induced Vibrations in Oil Well Drill Strings. *Multibody System Dynamics*, 23 (2), 191-207.
- Karnopp, D.C., Margolis, D. L., & Rosenberg, R. C., (2006). *System Dynamics; Modeling and Simulation of Mechatronics Systems*, 4<sup>th</sup> ed., New York: John Wiley & Sons, Inc.
- Khulief, Y. A., and Al-Naser, H., 2005. Finite Element Dynamic Analysis of Drillstrings. *Finite Element in Analysis and Design*, 41 (13), 1270-1288.
- Khulief, Y. A., Al-Sulaiman, F. A., and Bashmal, S., 2007. Vibration Analysis of Drillstrings with Self-excited Stick-slip Oscillations. *Journal of Sound and Vibration*, 299 (3), 540-558.
- Pavkovic, D., Deur, J., and Lisac, A., 2011. A Torque Estimator-based Control Strategy for Oil-well Drill-string Torsional Vibrations Active Damping Including an Auto-tuning Algorithm. *Control Engineering Practice*, 19 (8), 836-850.
- Sarker, M., Rideout, D.G., and Butt, S.D., 2012 "Advantages of an LQR Controller for Stick-Slip and Bit-Bounce Mitigation in an Oilwell Drillstring". *Proc. 2012 ASME International Mechanical Engineering Congress and Exposition, IMECE2012-87856*, November 9-15, Houston (Texas, USA).
- Serrarens, A. F. A., van de Molengraft, M. J. G., Kok, J. J., and van den Steen, L., 1998.  $H_{\infty}$  Control for Suppressing Stick-slip in Oil Well Drillstrings. *Control Systems, IEEE*, 18 (2), 19-30.
- Yigit, A. S., and Christoforou, A. P., 1996. Coupled Axial and Transverse Vibrations of Oilwell Drillstrings. *Journal of Sound and Vibration*, 195 (4), 617-627.
- Yigit, A. S., and Christoforou, A. P., 2006. Stick-slip and Bit-bounce Interaction in Oil-well Drillstrings. *Journal of Energy Resources Technology*, 128 (4), 268-274.
- Younesian, D. et al., 2010. Application of the Nonlinear Energy Sink Systems in Vibration Suppression of Railway Bridges. *Proc. ASME 10<sup>th</sup> Biennial Conf. on Eng. Sys. Design and Analysis*, July 12-14, Istanbul (Turkey).

## AUTHORS' BIOGRAPHIES

**Geoff Rideout** received his B.Eng. (Mechanical) from Memorial University of Newfoundland in 1993. After working in telecommunications equipment manufacturing and building systems consulting, he earned his M.A.Sc. in Mechanical Engineering from Queen's University in Kingston, Ontario and his Ph.D. in Mechanical Engineering from the University of Michigan. He has lectured at the University of Michigan and at the Humber Institute for Advanced Technology and Applied Learning in Toronto. He is currently Associate Professor at Memorial University, teaching mechanics, modeling, and design. His research areas are automated modeling, vibration-assisted drilling, vehicle dynamics and control, and modal testing for nondestructive evaluation.

**Farid Arvani** received his B.Sc. degree in Mechanical Engineering from University of Tabriz in 2003. He was actively involved in design and development of test facilities for condition monitoring and fatigue testing for the automotive industry for four years. He received his M.Eng degree in Mechanical Engineering from Memorial University of Newfoundland in 2009. He is currently a Ph.D. candidate and the Managing Engineer in the Advanced Drilling Project, an industry-driven research project at Memorial University focusing on the design and development of state-of-the-art technologies for the drilling industry.

**Stephen D. Butt** has B.Eng. and M.Sc. degrees from Memorial University of Newfoundland, a Ph.D. from Queen's University in Kingston, Canada, and is a registered Professional Engineer. From 1996 to 2006, he was a faculty member in the Faculty of Engineering at Dalhousie University, and has been a faculty member in Faculty of Engineering and Applied Science at Memorial University of Newfoundland from 2006 to the present, where he is currently Professor and Process Engineering Chair. He has held past administrative positions, including Mining Program Chair at Dalhousie University and Associate Dean at Memorial University. His research activities are in the area of drilling engineering, geomechanics and the development of geophysical imaging technology for various applications in petroleum, mining and civil engineering..

**Ehsan Fallahi** received his Bachelor's degree in Mechanical Engineering from Sharif University of Technology in Iran in 2010. His research interests are multibody dynamics and vibration problems in drilling. He is currently finishing his Master's degree in Oil and Gas Engineering at Memorial University.